6

A Polymer Physics View on Universal and Sequence-Specific Aspects of Chromosome Folding

Daniel Jost[1], *Angelo Rosa*[2], *Cédric Vaillant*[3], *and Ralf Everaers*[3]
[1]Université Grenoble Alpes, Grenoble, France [2]SISSA (Scuola Internazionale Superiore di Studi Avanzati), Trieste, Italy [3]Université Claude Bernard Lyon 1, Lyon, France

Recent advances in genome-wide mapping and imaging techniques have strikingly improved the resolution at which nuclear genome folding can be analyzed and have revealed numerous conserved features organizing the one-dimensional chromatin fiber into tridimensional nuclear domains. Understanding the underlying mechanisms and the link to gene regulation requires a crossdisciplinary approach that combines the new high-resolution techniques with computational modeling of chromatin and chromosomes. The present chapter discusses our current understanding of generic aspects of chromosome behavior during interphase. In particular, we present explanations from polymer physics for the emergence of the universal "territorial" folding of chromosomes *above* the Mbp scale and the sequence-dependent formation of *topologically associating domains* (TADs) *below* the Mbp scale.

6.1 Introduction

Eukaryotic genomes are partitioned into single, independent functional units, the chromosomes. Each chromosome contains a unique, polymer-like filament of double-helical DNA carrying the genetic information. Its total length can be measured in basepairs (bp) or, more commonly for very long chromosomes, thousands (kilo-basepairs, kbp) or millions of basepairs (mega-basepairs, Mbp). With a total of $\approx 7.0 \times 10^9$ bp split into 2×23 chromosomes, *Homo sapiens* is fairly typical for the estimated $(8.7 \pm 1.3) \times 10^6$ (Mora et al., 2011) species of eukaryotes currently living on our planet. Chromosome numbers range from

Nuclear Architecture and Dynamics. DOI: http://dx.doi.org/10.1016/B978-0-12-803480-4.00006-5

2×4 for *Drosophila* to 2×225 in a butterfly species (Lukhtanov, 2015) and reach the order of 1000 in some polyploid ferns (Leitch et al., 2005). Genome sizes are between $\approx 2.4 \times 10^7$ bp for budding yeast (*Saccharomyces cerevisiae*) and can reach $\approx 10^{11}$ bp in amphibians and flowering plants (Bennett and Leitch, 2005; Gregory, 2005). On the other hand, chromosome sizes can be either as small as ~ 0.2 Mbp in *S. cerevisiae* (http://www.ensembl.org/index.html) or as large as in the case of the Japanese plant *Paris japonica* where one single chromosome amounts to $\sim 4 \times 10^3$ Mbp (Pellicer et al., 2010).

For most of the time of the cell cycle, namely during the so-called *interphase* between cell divisions, the chromosomes of eukaryotic cells are confined to a specialized region, the nucleus (Alberts et al., 2007). Chromosome folding inside the nucleus is highly variable, but not random (Cremer and Cremer, 2001), and increasingly studied with visual and chromosome capture techniques (see, for instance, Weiland et al., 2011; Dekker et al., 2013; Shachar et al., 2015; Fraser et al., 2015a, 2015b and Part III of this book). In the present, brief review, we concentrate on features of interphase chromosomes, which can be understood in terms of the same theoretical and/or computational tools (Doi and Edwards, 1986; Grosberg and Khokhlov, 1994; Rubinstein and Colby, 2003; Kremer and Grest, 1990) which have been successfully applied to synthetic polymers and the related fields in soft matter physics (Grosberg, 2012; Halverson et al., 2014; Rosa and Zimmer, 2014). In particular, we present explanations from polymer physics for the emergence of (1) the universal "territorial" (Grosberg et al., 1993; Rosa and Everaers, 2008; Vettorel et al., 2009a, 2009b) folding of long chromosomes *above* the Mbp scale; (2) the sequence-dependent formation of *topologically associating domains*, the so-called TADs, *below* the Mbp scale (Dixon et al., 2012; Sexton et al., 2012). The manuscript is organized as follows: In Sections 6.2.1 and 6.2.2, we summarize relevant experimental observations, while the theoretical and modeling results are discussed in Sections 6.3 and 6.4. We conclude in Section 6.5 and discuss perspectives for future work.

6.2 Experimental Insight on Nuclear Genome Organization: From DNA to TADs and Chromosome Territories

To fix ideas and introduce the subject, consider the example of the human genome. The nuclei of human cells have a linear diameter of $\approx 10\,\mu$m and contain DNA with a total contour length of about 2 m (Alberts et al., 2007). Stretched out to their full extension of a few centimeters, the DNA of individual human chromosomes exceeds the diameter of the nucleus by more than three orders of magnitude. The association with histone proteins leads to compaction (Alberts et al., 2007). However, with a contour length in the millimeter range, the resulting *chromatin* fibers are still *strongly* folded when confined to the

nucleus (Emanuel et al., 2009). Owing to the refinement of experimental techniques, considerable progress has been made in recent years in investigating the nuclear structure and dynamics. In particular, biologists have now access to positions and distances (Cremer and Cremer, 2001), mobilities (Heun et al., 2001), and contact probabilities (Lieberman-Aiden et al., 2009) for (pairs of) specific genomic loci. Variations between *different* chromosomes, cell types, species in the spatial organization of the genome, and the response to specific environmental stimuli provide important *specific* insights into structural mechanisms of genome activity regulation. In contrast, the generic (i.e., sequence independent) chromosome behavior emerges by averaging experimental data over different genomic sequences or between different cells.

6.2.1 Universal Aspects of Chromosome Folding

During interphase, chromosomes decondense and appear to lose their identity. However, confirming (Cremer and Cremer, 2006) pioneering observations by Rabl (1885) dating back to the ending of the 19th century, chromosome labeling by *Fluorescence in-situ Hybridization* (FISH) has revealed a remarkable universal motif in nuclear organization: chromosomes occupy distinct *territories* and do not mix (Cremer and Cremer, 2001). [Some notable exceptions have been described. For instance, detection of territories in organisms with small genomes like yeast has appeared to be elusive (Haber and Leung, 1996). Yet, some "loose" territoriality at the gene level has been reported (Berger et al., 2008).] Disregarding sequence effects and considering chromosome folding as a function of genomic distance reveals additional interesting features (Fig. 6.1). In panel A, we show a compilation of experimental data for the mean-square spatial distance, $\langle R^2(N_{\mathrm{bp}})\rangle$ as a function of the number of base pairs (bp), N_{bp}, separating two sites along a chromosome. Panel B contains *sequence-averaged* contact probabilities, $p_c(N_{\mathrm{bp}})$. All biological specificity is suppressed: In fact, data for yeast and human chromosomes nicely superpose on corresponding length scales (around 0.1 Mbp). Moreover, and as often in polymer physics, the data exhibit power-law behavior with $\left\langle R^2(N_{\mathrm{bp}})\right\rangle \propto N_{\mathrm{bp}}^{2\nu}$ and $p_c(N_{\mathrm{bp}}) \propto N_{\mathrm{bp}}^{-\gamma}$ characteristic of fractal structures (Rubinstein and Colby, 2003). But unlike textbook (Doi and Edwards, 1986; Grosberg and Khokhlov, 1994; Rubinstein and Colby, 2003; De Gennes, 1979), polymers in concentrated solutions where $\nu = 1/2$ and $\gamma = 3/2$, the large-scale behavior of long chromosomes seems to be characterized by "noncanonical" exponents $\nu \approx 1/3$ (Münkel et al., 1999) and $\gamma \approx 1$ (Lieberman-Aiden et al., 2009) (Fig. 6.1). In Section 6.3, we will rationalize these observations in terms of a coherent theoretical framework based on polymer physics.

6.2.2 Sequence-Specific Aspects of Chromosome Folding

In recent years, genome-wide chromosome conformation capture techniques (HiC; Lieberman-Aiden et al., 2009) have revealed reproducible, sequence, and epigenetic state dependent features in the nuclear organization of chromatin,

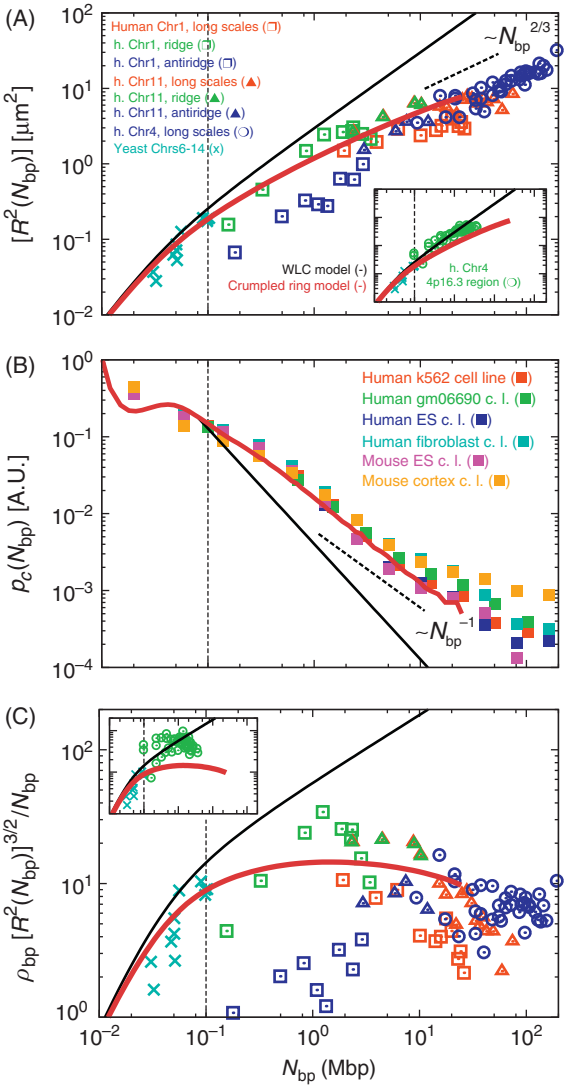

Figure 6.1 Experimental behavior of interphase chromosomes (symbols) compared to generic polymer models (solid lines). (A) Mean-square internal distances, $\langle R^2(N_{bp})\rangle$, between genomic sites separated by N_{bp} Mbp along the chromatin fiber: experimental results for interphase yeast (Bystricky et al., 2004) and human chromosomes (Sachs et al., 1995; Mateos-Langerak et al., 2009) obtained by FISH (symbols), compared to the WLC model (black line) and the crumpled ring model (red line, Rosa and Everaers, 2014). The inset reproduces FISH data from the "equilibrated" 4p16.3 terminal region on human chromosome 4 (Rosa and Everaers, 2008). The crumpled ring model deviates only from data for the antiridge region on human chromosome 1. (B) Average contact probabilities between genomic sites: experimental results for human and mouse chromosomes in different cell lines measured by HiC (Dixon et al., 2012; Lieberman-Aiden et al., 2009) (symbols), and corresponding predictions for the WLC model and the crumpled ring model (solid lines). (C) Overlap parameters corresponding to the data shown in (A). Taken together, these data are consistent with expected deviations from the ideal WLC behavior (black lines) occurring in the "bulk" of eukaryotic chromosomes when $\frac{\rho_{bp}}{N_e}\langle R^2(N_e)\rangle^{3/2} \equiv 20$, with $N_e \approx 10^5$ bp (vertical dashed lines).

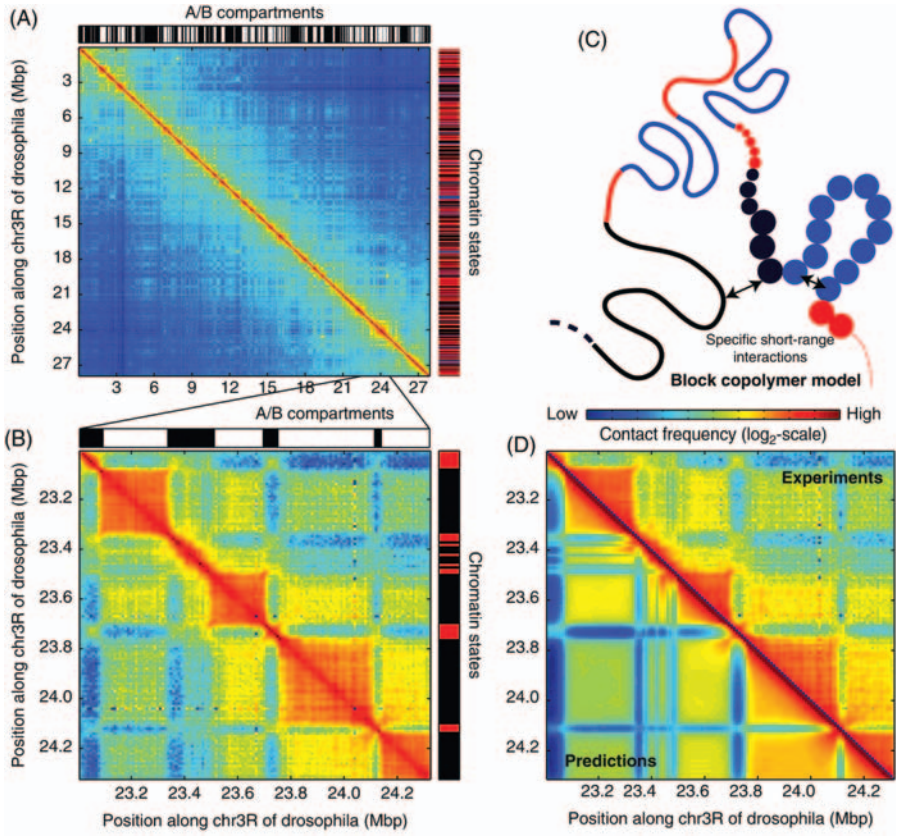

Figure 6.2 (A) Contact frequency map across chromosome 3R of *Drosophila melanogaster* based on HiC data (Sexton et al., 2012) at 30 kbp bin size. The checkerboard-like pattern of long-range contacts allows the definition of two compartments A and B (black and white segmentation at the top). The local chromatin states (Ho et al., 2014) are given at the right-hand side (red for active, blue for facultative heterochromatin, green for constitutive heterochromatin and black for null heterochromatin). (B) Zoom on the 23–24.3-Mbp region at 10-kbp bin size showing the local segmentation into TADs. (C) Block copolymer model of chromatin: each monomer is characterized by a chromatin state. Short-range-specific interactions are considered between monomers of the same state. (D) Illustration of the predictive outcome of the copolymer model for the region displayed in (B).

at the subchromosomal ($\lesssim$1 Mbp) scale (Fig. 6.2A). They are interpreted as a 3D segmentation into TADs characterized by an enrichment of intradomain contact frequencies and a partial 3D insulation between adjacent domains (Fig. 6.2B) (Dixon et al., 2012; Nora et al., 2012). Their sizes vary from few kbp up to Mbp. TADs are observed in many species ranging from yeast to human (Sexton and Cavalli, 2015) and have been shown to be conserved during

cellular differentiation (Dixon et al., 2015) and even between close species (Dixon et al., 2012; Rao et al., 2014). At larger scales, HiC maps of higher eukaryotes display a characteristic cell-type-specific checker-board-like pattern where TADs engage in long-range interactions (Fig. 6.2A) (Lieberman-Aiden et al., 2009). Statistical analysis of the local enrichment (or depletion) of contacts compared to the average behavior has demonstrated the presence of two main compartments (often named A and B) that partition the genome at a higher scale: Contacts between genomic regions or TADs belonging to the same compartment are more frequent than between regions of different ones (Lieberman-Aiden et al., 2009; Imakaev et al., 2012). In general, the A compartment is mainly composed of active—euchromatic—regions, while B is more repressed and heterochromatic. These compartments may eventually be subdivided into subcompartments, characterizing substates of the chromatin (Sexton et al., 2012; Rao et al., 2014). This highlights the strong correlation between the global 3D chromatin organization and the local activities or states of the chromatin (Sexton et al., 2012; Ho et al., 2014; Fraser et al., 2015a, 2015b; Zhu et al., 2016).

A key question concerns the mechanisms behind the formation of TADs and compartments. Again, polymer physics may be a powerful tool to build minimal models for investigating the validity of proposed processes. In Section 6.4, we will discuss the role of specific interactions in *hetero*polymer models, which can selectively stabilize some of the transiently appearing branched loop structures from the generic *homo*polymer models to be discussed in Section 6.3.

6.3 Universal Aspects of Chromosome Folding: Polymer Theory

We begin our analysis with the large scale, generic features of chromosome folding summarized in Section 6.2.1. This choice is not obvious. Physical modeling proceeds from small to large scales and one might be tempted to dismiss the generic features as a "vague echo" of biologically relevant structures, which are defined through contacts between specific genomic sites and which are maintained by a complex, evolved molecular machinery. The fractal nature of the chromosome conformations would then be a mere curiosity. Instead, we adopt (and explain) the opposite point of view that sequence averaging reveals the *generic*, polymer-like structure and dynamics of interphase chromosomes. We show that the available experimental evidence for their behavior can be *quantitatively* predicted by maximizing the entropy of a chromatin fiber model under the constraint that chromosomes are free of knots and not entangled with each other (red solid lines in Fig. 6.1). As a consequence, and as largely emphasized at the end of Section 6.2.1, the emerging picture of the folding of interphase chromosomes departs from the "traditional" one for linear chains in equilibrated solutions or melts (Doi and Edwards, 1986; De Gennes, 1979). In

particular, we believe that the proper modeling of topological constraints and the largely knot-free microscopic topological state of interphase chromosomes prior to replication represent an essential feature of models for sequence-specific aspects of chromosome folding.

6.3.1 Chromatin Fiber Entanglement

Given the controversial fiber structure (Maeshima et al., 2010) and the complexity of chromatin on the molecular scale, it is far from obvious, that polymer physics has relevant qualitative or even quantitative insights to offer. A polymer model characterizes chains by their contour length, L, and their Kuhn length, l_K, as a measure of the chain stiffness. For contour lengths $L \ll l_K$, thermal fluctuation have little effect, and the chains are effectively rigid with mean square end-to-end distances $\langle R^2(L)\rangle = L^2$ and $\nu = 1$. For $L \gg l_K$, equilibrated linear chains exhibit random coil statistics with $\langle R^2(L)\rangle = l_K\, L$ and $\nu = 1/2$. In this regime, the contact probability, p_c, between two segments scales like $p_c(L) \sim (L = l_K)^{-\gamma}$ with $\gamma = 3\nu = 3/2$. The crossover for $L \approx l_K$ can be conveniently described by the worm-like chain (WLC) model (Kratky and Porod, 1949; Becker et al., 2010), excluded volume interactions being screened in concentrated solutions (Doi and Edwards, 1986). For 30-nm chromatin fibers, $L = 0.01 N_{\mathrm{bp}}$ nm and $l_K \approx 300$ nm (Bystricky et al., 2004). For the locally much less compact 10 nm fibers, a simple estimate [The nucleosome core particle (i.e., the histone octamer plus the wrapped DNA) has a roughly cylindrical shape with a diameter of 10 nm and a height of 6 nm (Luger and Hansen, 2005). With around 50 bp per linker, the typical distance between the centers of neighboring core particles is of the order of "10 nm + (50 bp)/(3 bp/nm) = 25 nm." The contour length density of the 10-nm fiber is hence "(200 bp)/(25 nm) = 8 bp/nm." Allowing for variations in the linker length (a variation of "$\pm$1 bp" corresponds to a rotation of $\pm 34^\circ$ around the linker axis due to the twist of the double-helix) (Yao et al., 1990), for over- and underwrapping of DNA in the core particle as well as for the conformational flexibility of the linkers, subsequent "bond vectors" between core particle centers are to a first approximation uncorrelated. In this case, the Kuhn length of the 10-nm fiber equals $l_{K;10\mathrm{nm}} = 25$ nm.] assuming uncorrelated orientations of subsequent nucleosomes yields $L = 0.125 N_{\mathrm{bp}}$ nm and $l_K \approx 25$ nm. Interestingly, the two fiber models predict with $\langle R^2(N_{\mathrm{bp}})\rangle \approx 3 N_{\mathrm{bp}}$ nm^2 identical mean-square internal distances in the random walk regime for genomic distances larger than 30 kbp, suggesting that this estimate should be relatively robust and even apply to fibers, whose local structure alternates between dense 30 nm and open 10 nm conformations (Florescu et al., 2016). As shown in Fig. 6.1A and B, the predictions of the WLC model (black lines) are in reasonable agreement with the sequence-, cell-type, and species-averaged experimental data for genomic distances up to $\approx$100 kbp and, in exceptional cases such as equilibrated telomeric regions (Rosa and Everaers, 2008), even on the Mbp scale.

Similarly to macroscopic strings tied into knots, diffusing polymer chains can slide past each other, but their backbones cannot cross. The resulting

topological constraints (Edwards and Phys, 1967; Prager and Frisch, 1967) start to affect polymers beyond the so-called entanglement length, N_e (Doi and Edwards, 1986). According to the packing argument for loosely entangled chains (Kavassalis and Noolandi, 1987; Fetters et al., 1994; Uchida et al., 2008), N_e can be determined from the condition that the so-called overlap parameter, $\Omega(N_{\mathrm{bp}}) \equiv \frac{\rho_{\mathrm{bp}}}{N_{\mathrm{bp}}}\langle R^2(N_{\mathrm{bp}})\rangle^{3/2}$, reaches a characteristic threshold, $\Omega \equiv 20$ (Rosa and Everaers, 2014; Kavassalis and Noolandi, 1987; Fetters et al., 1994; Uchida et al., 2008). For typical nuclear densities of $\rho_{\mathrm{bp}} \approx 0.011$ bp/nm^3, both fiber models suggests an entanglement length for genomic DNA of the order of (Rosa and Everaers, 2008)

$$N_e = 1.2 \times 10^5 \mathrm{bp}. \tag{6.1}$$

Note, however, that this crucial length scale is strongly density dependent (Halverson et al., 2014; Uchida et al., 2008). The relevance of topological constraints for the structure of chromosomes can be verified directly from the experimental data. In panel 6.1C, we have plotted dimensionless packing ratios inferred from FISH data. Comparison with panels 6.1A and 6.1B shows that deviations from the WLC behavior set in on length scales, where the overlap parameter approaches the entanglement threshold of 20. Qualitatively, the constant overlap parameter on large scales is compatible with a $\nu \approx 1/3$ regime, where the chain extension is controlled by the entanglement threshold. The corresponding time scale for the onset of entanglement effects, $\tau_e \approx 32$ s, can be estimated (Rosa and Everaers, 2008) by reinterpreting the anomalous diffusion of a fluorescently labeled site (Cabal et al., 2006) in terms of the characteristic slowing down of the polymer motion on the entanglement scale.

6.3.2 Chromosome Conformations as Crumpled, Randomly Branched Ring Polymers in Solution

For *linear* chains, topological constraints are transient. Typically, they dominate the viscoelastic behavior of long-chain melts or solutions (Doi and Edwards, 1986; McLeish, 2002), but do not affect the *equilibrium* statistics as the systems remain ergodic. However, this may not be taken for granted in the case of chromosomes. With entanglement times, τ_e, in the range of minutes and an effective size of $Z = N_{\mathrm{bp}}/N_e = 1000$ entanglements, equilibration of the microscopic *topological* state via reptation (De Gennes, 1971) is expected (Rosa and Everaers, 2008; Sikorav and Jannink, 1994) to require centuries as $\tau_{\mathrm{max}} = Z^3\tau_e$. As a consequence, the *topological state* of interphase chromosomes prior to replication is not random but *identical* to the topological state during the preceding metaphase step of the cell cycle. In particular, there are no topological *links* between different chromosomes.

Grosberg et al. (1993) were the first to argue along these lines, that chromosomes should be in an essentially unknotted state to perform their function.

In particular, they suggested that due to topological constraint, chromosomes should fold and interpenetrate differently from polymers in equilibrated melts or semidilute solutions. To describe such conformations, they drew an analogy to crumpled globules resulting from the rapid collapse of an isolated polymer chain, which initially preserve the (nearly) unknotted topological state of the good solvent conformation (Grosberg et al., 1988). Recently, this view received strong support from the interpretation of their HiC data by Lieberman-Aiden et al. (2009), even though the analogy, when taken too literally, does not seem to lead to well-defined structures (Schram et al., 2013).

As an alternative, two of us (R.E. and A.R.) considered (Rosa and Everaers, 2008) the opposite process of decondensing initially unknotted and spatially separated (and hence topologically unlinked) metaphase chromosomes in solutions with concentrations corresponding to interphase nuclei. Using a carefully mapped, parameter-free model of chromatin fibers, we were able to reproduce the experimental data (Rosa and Everaers, 2008; Rosa et al., 2010). In particular, we were able to show that the bulk of our linear model chromosomes exhibited the same behavior as corresponding *equilibrated*, semidilute solutions of *un*entangled *ring* polymers, which show the same "territorial" behavior as interphase nuclei (Vettorel et al., 2009a, 2009b).

Understanding this behavior has been a long-standing problem in polymer physics (Grosberg, 2012, 2014; Rosa and Everaers, 2014; Grosberg et al., 1988; Vettorel et al., 2009a, 2009b; Khokhlov and Nechaev, 1985; Cates and Deutsch, 1986; Klein, 1986; Rubinstein, 1986; Brereton and Vilgis, 1995; Müller et al., 1996, 2000; Suzuki et al., 2009; Halverson et al., 2011). Khokhlov and Nechaev (1985) and Rubinstein (1986) were the first to argue that such rings should adopt randomly branched, doubled-folded conformations, which reduce the threadable surface they present to each other. Fig. 6.3

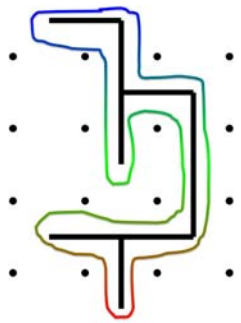

Figure 6.3 Illustration of a randomly branched ["lattice tree"-like (Rosa and Everaers, 2014)] ring conformation (rainbow-colored line) with topological constraints ideally represented as an array of fixed obstacles (black dots, see De Gennes, 1971; Obukhov et al., 1994). In reality, topological constraints are not permanent as they are constituted by surrounding rings which are all subjected to the same stochastic Brownian motion.

illustrates the notion of topologically constrained, randomly branched ring conformations. In a recent study (Rosa and Everaers, 2014), two of us (R.E. and A.R.) have validated this idea by developing it into a quantitative multiscale approach, where a computationally efficient Monte-Carlo method is used to generate branched polymer conformations (Rosa and Everaers, 2016), which are subsequently "fine-grained" to corresponding off-lattice conformations of *nonconcatenated and unknotted* rings for the fiber model. While the generated conformations are in excellent agreement with the results of brute-force equilibration for $Z \sim 100$, the multiscale approach provides access to much larger system sizes.

As in our original study (Rosa and Everaers, 2008), all results can be quantitatively mapped to experimental data for chromatin. With $M = 64$ rings of length $Z_r = 900$, our largest systems are comparable in size to the nucleus of a human cell (Fig. 6.4). Fig. 6.4A illustrates the characteristic segregation of ring polymers and qualitatively reproduces (Rosa and Everaers, 2008; Vettorel et al., 2009a, 2009b) chromosome territories (Cremer and Cremer, 2001). Remarkably, Fig. 6.1 demonstrates (red lines) that our parameter-free model quantitatively reproduces the available FISH (Bystricky et al., 2004; Sachs et al., 1995) and conformation capture data (Dixon et al., 2012; Lieberman-Aiden et al., 2009). Similarly, the reported aspect ratios of chromosome territories of 4.5:2.9:1.0 (Khalil et al., 2007) closely agree with asymptotic values of 4.9:1.9:1.0 from the (interacting) lattice tree model. The effective exponents $\nu = 0.32 \pm 0.01$ and $\gamma = 1.11 \pm 0.01$ we observed in this regime agree with the reported behavior of interphase chromosomes.

Two length scales emerge. First, branching sets in on the entanglement scale of $\sim$100 kbp. Interestingly, this is in excellent agreement with the average size of chromatin loops regulated during meiosis (Heng et al., 1996), and with typical genomic distances between enhancers and corresponding transcription start sites, as reported in a recent study employing chromosome conformation capture techniques (Sanyal et al., 2012). Second, the structures become locally compact (Fig. 6.1A) on the scale of $\sim$1 Mbp or $Z \sim 10$ entanglements, i.e., on the TAD scale. Fig. 6.4B and C illustrates that the territorial segregation also persists inside chromosomes down to this scale, but not below. As anticipated by Grosberg et al. (1993, 1988), our results for ring polymers (Rosa and Everaers, 2014) are relevant to linear chromosomes due to a separation of time scales (Rosa and Everaers, 2008) illustrated in Fig. 6.5: the times scale for the relaxation of the microscopic topological state of human chromosomes [of the order of centuries, estimated as $\tau_e Z_{\mathrm{chr}}^3$ (Rosa and Everaers, 2008; De Gennes, 1971; Sikorav and Jannink, 1994) as a function of the *total* chromosome size $Z_{\mathrm{chr}} = \mathrm{O}(10^3)$ or $N_{\mathrm{chr}} = 10^8$ bp] far exceeds the time required for the *structural* relaxation of a topologically constrained chromosome on local scales $Z \leq Z_{\mathrm{chr}}$ [estimated as $\tau_e Z^{5/2}$ in the ideal lattice tree regime (Obukhov et al., 1994) and estimated from relaxation times in Molecular Dynamics simulations

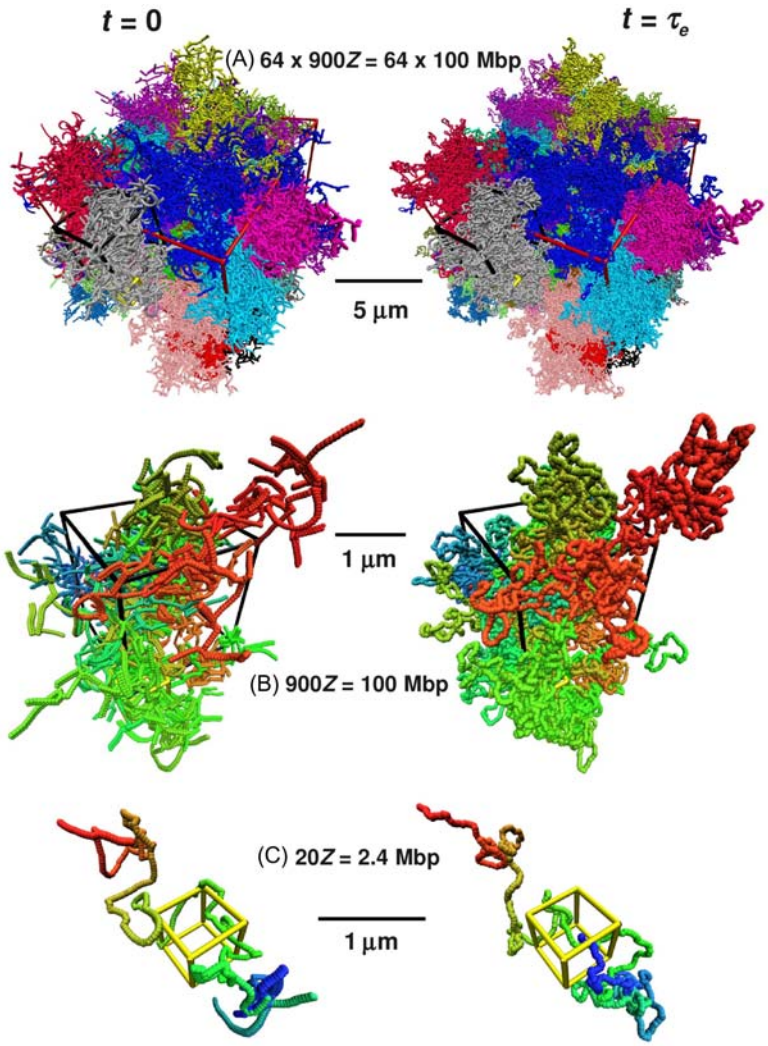

Figure 6.4 (A) Model conformations of 64 *interacting* ring polymers, described by the lattice tree model with excluded volume interactions (Rosa and Everaers, 2014). The contour length of each ring is $N_r = 108$ Mbp or $Z_r \equiv N_r/N_e = 900$, corresponding to the typical size of a human (mammalian) chromosome. (B) Single-ring conformation. (C) Ring portion from the single-ring conformation in (B), corresponding to $Z = 40$. Boxes indicate the volume, $\left(\frac{\rho_{bp}}{N_r}\right)^{-1}$ available to corresponding configurations at the nominal chromatin density, $\rho_{bp} = 0.011$ bp/nm^3 (Rosa and Everaers, 2008).

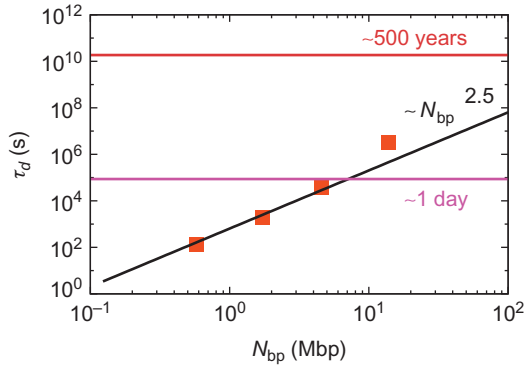

Figure 6.5 Time scales separation between equilibration times of ring polymers (red symbols, well described by the $N_{bp}^{5/2}$-power-law behavior predicted by Obukhov et al., 1994) and the estimated (Rosa and Everaers, 2008) 500-years reptation time of long, linear polymer chains the size the human chromosomes ($N_{bp} \approx 100$ Mbp, red line). One day (magenta line) is the typical time scale of the cell cycle for most animal cells (Alberts et al., 2007).

of our fiber model]. In particular, we find that during the typical length of a cell cycle of $\approx$24 hours (Alberts et al., 2007) the local equilibration of chromosomes structure should also proceed up to the $\approx$Mbp scale.

To summarize, the structures emerging from topological constraints in noncatenated ring melts share many generic features of interphase chromosomes. The chains may be said to be *crumpled* (Grosberg et al., 1993, 1988), to exhibit a form of random looping (Mateos-Langerak et al., 2009; Bohn and Heermann, 2010), and to segregate in subcompartments (Münkel et al., 1999). There are similarities to the crumpled or fractal globule model of chromosomes (Grosberg et al., 1993; Lieberman-Aiden et al., 2009; Rosa and Everaers, 2014), but also important differences in that the absence of surface tension in the many-chain system leads to strongly interpenetrating, aspherical territories. As these phenomena spontaneously *emerge* in suitable polymer models (Rosa and Everaers, 2008), the approach can *explain* rather than *describe* generic features of interphase chromosomes, *quantitatively* predict the emerging characteristic length scales, and be *integrated* into more detailed models addressing sequence-specific aspects of chromosome folding.

6.4 Sequence-Specific Aspects of Chromosome Folding: Polymer Theory

Our ability to predict the sequence-averaged structure suggests that we have reached a quantitative, physical understanding of *one* important aspect of

chromosome folding. However, the discussion presented in Section 6.2.2 clearly points out that there are many aspects in chromosome biology, which are intimately connected to the DNA sequence. Motivated by the observed correlations between the 1D chromatin states and the 3D chromatin organization, heteropolymer models have started to emerge which explicitly consider the coupling between chromatin structure and function (Barbieri et al., 2012; Jerabek and Heermann, 2012; Brackley et al., 2016; Benedetti et al., 2014; Doyle et al., 2014; Ganai et al., 2014; Jost et al., 2014; Tark-Dame et al., 2014; Nazarov et al., 2015; Sanborn et al., 2015; Ulianov et al., 2016; Fudenberg et al., 2016; Tiana et al., 2016; Chiariello et al., 2016). These models posit that chromatin folding might likely be driven by direct or effective specific short-range interactions between genomic loci. While the existence of effective interactions in heterogeneous polymers is well established (Bates and Fredrickson, 1990), the microscopic foundations of these interactions are still unclear but, in the case of chromatin, may originate from (1) local direct chromatin–chromatin interactions mediated by chromatin-binding proteins with sequence- or epigenetic-specific affinities (Canzio et al., 2013; Isono et al., 2013; Hiragami-Hamada et al., 2016), "block copolymer" model (Jost et al., 2014), or "binder" models (Barbieri et al., 2012; Brackley et al., 2016); (2) chromatin fibers with different local packing ratios ["10/30 nm"-mixed-fibers model (Florescu et al., 2016)] depending for example on epigenetics or gene activity (Allis et al., 2007); (3) nonthermal active (ATP-consuming) processes like transcription or chromatin remodeling (Weber et al., 2012) ["activity-based segregation" model (Ganai et al., 2014)].

In the following, we are going to focus on some recent ideas (Jost et al., 2014; Olarte-Plata et al., 2016) concerning the connection between polymer physics and the formation of sub-Mbp domains (TADs) inside chromosome territories. Chromatin is modeled as a block copolymer where blocks corresponds to consecutive monomers with an identical chromatin state (Fig. 6.2C). The dynamics of the chain is then controlled by thermal fluctuations, excluded volume, eventually bending rigidity of the fiber, and attractive short-range interactions between monomers of the same state.

In *Drosophila melanogaster*, two of us (C.V. and D.J.) have extensively studied the behavior of such model at the Mbp scale (Jost et al., 2014; Olarte-Plata et al., 2016) (Fig. 6.2D). As explained in Section 6.3, systems can structurally equilibrate at this scale and we neglected topological constraints in the crossover regime to territorial behavior. Numerical investigations of the block copolymer were performed using either standard Molecular dynamics or kinetic Monte-Carlo simulations or an efficient self-consistent Gaussian approximation (Jost et al., 2014; Ramalho et al., 2013). The qualitative behavior of the system is independent of the chosen method. By varying the strength of specific interactions, the systems exhibit a variety of different phases (Fig. 6.6). For weak interactions, configurations are characteristic of

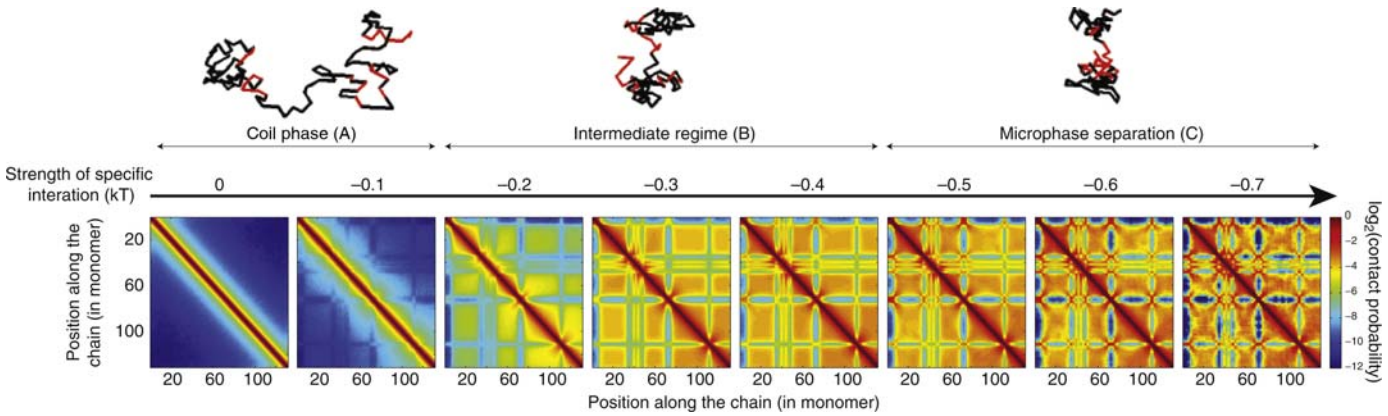

Figure 6.6 Contact frequency maps predicted by the copolymer model for the genomic region of *Drosophila* displayed in Fig. 6.2B, obtained by varying gradually the strength of specific interactions between monomers of the same state. System varies continuously from an unstructured, coil phase (A) to a microphase separation (C), exhibiting an intermediate regime (B) consistent with HiC experiments (Fig. 6.2D). For each phase, snapshots of typical configurations are shown. Results were obtained using kinetic Monte-Carlo simulations of a polymer lattice model (see Olarte-Plata et al., 2016).

an unstructured, coil phase (Fig. 6.6A). For strong attractive interactions, a microphase separation is observed and large portions of monomers of the same state occupied separate spatial compartments leading to strong checker-board patterns (Fig. 6.6C). In the intermediate regime, the system exhibits a continuous crossover between the coil and the microphase regimes (Fig. 6.6B). We observe the partial internal collapse of blocks into TAD-like domains, followed by the appearance of weak long-range stochastic interactions between TADs of the same chromatin state. The corresponding 3D compartments may contain several TADs but are transient and only weakly collapsed. As the interactions become more attractive, the blocks experience an internal θ-collapse transition to an equilibrium globule and long-range interactions become more and more important, leading to the formation of long-lived larger 3D compartments. The precise shape of the phase diagram, as well as the behavior of individual blocks, is strongly dependent on the underlying pattern of chromatin states (size of blocks, number of different states, etc.) (Jost et al., 2014; Olarte-Plata et al., 2016). For example, larger blocks will start collapsing at weaker interaction strength due to stronger collective effects (Olarte-Plata et al., 2016).

Experimental HiC data, with their evidence of the formation of TADs and A/B compartments, are compatible with the intermediate regime (Fig. 6.2D) where chromatin blocks have partially collapsed into TADs and where blocks of the same state transiently merge together into dynamic 3D compartments resulting in the characteristic weak checker-board pattern of A and B compartments observed in HiC maps. This observation is consistent with FISH microscopy experiments of Polycomb bodies, spatial compartments associated with facultative heterochromatin, showing that such bodies are indeed highly dynamic inside the fly nucleus (Cheutin and Cavalli, 2012). In this intermediate regime, prediction of the time-evolution of the contact maps shows that TADs form quickly first, followed by the slow formation of long-range interactions. This is again in agreement with HiC data on synchronized cells along the cell cycle (Naumova et al., 2013). Another property of systems in this regime is the internal compaction of TADs that increases with the TAD size for a given interaction strength. In *Drosophila*, this simple prediction agrees nicely with the measurements on heterochromatic TADs (Olarte-Plata et al., 2016; Boettiger et al., 2016). Interestingly, for active(euchromatic)domains, the compaction does not depend on the size, again pointing out that active chromatin only weakly interacts with itself. This may reflect a distinct local mode of interaction between chromatin types: active chromatin rather organizes locally via pairwise short-range bridging between discrete specific genomic sites, while heterochromatin may interact more continuously via clustering of multiple chromatin loci. This is consistent with more homogeneous internal contact patterns observed for inactive domain and more complex interactome profiles for active domains (Sofueva et al., 2013).

6.5 Discussion and Conclusions

In this chapter, we have summarized the results of our collective efforts to understand chromosome folding in terms of polymer physics. In particular, we have discussed the physical origin of

1. The experimentally observed territorial (Section 6.2.1) chromosome structure. In our framework, universal aspects of chromatin folding may be understood by the thermal (Brownian) relaxation of topologically constrained chromatin fibers. Nuclei resemble solutions of densely packed unknotted and unentangled ring polymers which form highly branched conformations (Section 6.3).
2. The formation and structure of interaction domains and compartments. Here, they arise as the consequence of the self-organization and microphase separation of chromatin clusters growing inside a model copolymer with sequence-specific chromatin–chromatin interactions (Section 6.4). The model reproduces with remarkable accuracy the check-board pattern of contact matrices from HiC experiments in *D. melanogaster* (Section 6.2.2).

While the reported agreement with available experimental data is very encouraging, the two proposed approaches do not pretend to be exhaustive or give a complete explanation to chromosome structure. What is currently missing, which should be also considered as a promising direction for future work?

First, to what concern the *large-scale* ($\gtrsim$1 Mbp) structure of chromosomes, we should ask if our computational approach is pertinent in the presence of intra- and interchromosomal contacts, of confinement by and attachment to the nuclear membrane and matrix (Pederson, 2000), or of transcriptional activity. Is it really adequate, to either neglect these features or to view them not as being designed to cause looping, but as stabilizing the large-scale conformation of chromatin fibers, which generically adopt fluctuating branched loop structures? The topological constraints lead to the confinement of chromosomes to territories, which are one order of magnitude *smaller* than the nucleus. This key aspect is thus properly represented in bulk studies at the nuclear density. Neglecting confinement is nevertheless an approximation. In nuclei with a few dozen chromosomes, none is very far from the nuclear membrane, even though this finite size effect should be less critical for the chromosome structure on smaller scales. Concerning transcriptional activity, the generic structure and the absence of long-lived entanglements strike us as a *prerequisite* for the activity (and evolution) of transcription factories (Cook, 1999), rather than a consequence (Cook, 2010) resembling self-organized active structures in the cytoskeleton (Nedelec et al., 1997). We want to stress here, that by all this, we do *not* mean to imply that the nuclear architecture of biological organisms can be understood neglecting transcriptional activity, confinement by and attachment to the nuclear membrane and matrix, intra- and interchromosomal

contacts and, in particular, the evolved *specificity* distinguishing organisms and cell lines. We rather propose to view them as *stabilizing* the large-scale conformation of dynamically branched loop structures of chromatin fibers rather than as having evolved *to create* looped equilibrium structures in linear chains in an origami-like (Rothemund, 2006) fashion. In this respect, we suggest then that some care should be required in addressing the role of specific interactions between different genomic sites or linking chromosomes at designated points to the nuclear membrane and or a nuclear matrix (Pederson, 2000).

To conclude this part of the discussion, we believe that topological constraints constitute an *essential* feature to be retained in *minimal* models. These examples illustrate that the discussion of the origin of the generic structure is far from academic. Instead, a quantitative understanding of the interaction free "null model" is essential for attempts to reconstruct or predict the three-dimensional structure (Wong et al., 2012; Baù et al., 2011) or the dynamics of entire cell nuclei. Given an initial conformation of chromosomes (e.g., Rabl-like in *Drosophila*), and any other known large-scale geometrical "static" constraint [e.g., shape of the nucleus, anchoring of centromeres (Wong et al., 2012), etc.] and, given a proper mapping of the simulation vs real time, such "null-models" are likely to provide a description of the large-scale structure and dynamics of nuclear compartmentalization.

Second, regarding the *small-scale* ($\lesssim$1 Mbp) structure of chromosomes, we stress once again that our experimentally motivated working hypothesis that 3D chromatin organization is driven by short-range-specific interactions between genomic regions sharing the same chromatin state has mainly been quantitatively investigated in *Drosophila*. As a matter of fact, it is still questionable in higher vertebrates like mammals. On this point, it has been reported recently that about half of the TADs in mammals contain strong loops between oriented CTCF sites usually located at the two boundaries of the domain (Rao et al., 2014). While the formation of such loops can still be explained using the same class of models (Brackley et al., 2016; Sanborn et al., 2015; Chiariello et al., 2016), the pivotal observation that looping mainly occurs between convergent CTCF sites (Rao et al., 2014) is incompatible with short-range interactions (Sanborn et al., 2015; Fudenberg et al., 2016). Recently, it was shown that such observations are consistent with an active extrusion mechanism (Sanborn et al., 2015; Fudenberg et al., 2016). Protein complexes, putatively cohesins or condensins, bind to chromatin and extrude sequentially large DNA loops before eventually unbinding or stopping at specific loci like CTCF sites having the proper orientation. This model suggests that the local 3D organization is controlled by the presence and orientation of 1D barriers. Polymer models implementing this mechanism have shown that TAD formation and loop interaction at the corners of the domains could be explained by the extrusion process. Moreover, such models can quantitatively predict the perturbed 3D organization after deletion, inversion or duplication of CTCF sites (Nora et al.,

2012; Sanborn et al., 2015; Lupiáñez et al., 2015; Guo et al., 2015). They also provide a very elegant mechanism for the formation of mitotic chromosomes and for the separation of sister chromatids, arising from an increase in the number of loop extruders coupled to a decrease in the number of boundary elements (Goloborodko et al., 2016a, 2016b). However, loop extrusion cannot account for long-range communications between TADs, for the formation of the A/B compartments or for interactions with the nuclear membrane that are likely to be driven by genomic or chromatin-associated information. Heteropolymer models accounting for both loop extrusion and specific short-range interactions remain to be developed in order to quantitatively describe within the same framework the local and higher order chromosome organization in mammals.

Interestingly, a still open question is if the spatial organization of chromatin resulting (in part) from the clustering of chromatin states is only a *by-product* of genome activity or is actively participating to the local regulation of the chromatin assembly and more generally to the regulation of the genome function. An attractive hypothesis is that 3D domains (TADs, A/B compartments) would correspond to nanoreactors: a few number of chromatin-associated complexes colocalizes in space, increasing their local concentration and thus promoting their biochemical activity on chromatin. Nucleation by a small number of factors coupled to self-assembly or multimerization of biomolecules leads to the formation of interaction domains which further enhance, stabilize, and/or perpetuate the active or repressed environment. TADs would correspond to subreactors, having a role in either preventing or facilitating the communication between distal regulatory genomic elements at the sub-Mbp scale thus enhancing efficiency of gene coactivations or corepressions (Sexton and Cavalli, 2015; Tolhuis et al., 2011). Domain sizes through the control of global compaction may have coevolved in order to increase the robustness of these regulatory contacts, for example to motif mutations (Sexton and Cavalli, 2015). The (self-) assembly of TADs into A/B compartments is a softer mode of regulation where spatial confinement increase binding affinities to the regulated sequences. Development of mixed models coupling the heteropolymer description to standard gene or epigenetic regulation dynamics (Wilkinson, 2009; Dodd et al., 2007; Jost, 2014) would certainly be very helpful in the near future to theorize and quantify such concepts but also to interpret more deeply experimental observations.

Acknowledgments

We thank Peter Meister and Giacomo Cavalli for fruitful discussions. We acknowledge our funding agencies: Agence Nationale de la Recherche (ANR-15-CE12-0006 EpiDevoMath; D.J./C.V./R.E.), Fondation pour la Recherche Médicale (DEI20151234396; D.J./C.V.), CNRS (D.J./C.V.), Institut Rhône-Alpin des Systèmes

Complexes (D.J.), program AGIR of University Grenoble Alpes (D.J.), ENS de Lyon (C.V./R.E.), Italian Ministry of Education (PRIN 2010HXAW77; A.R.), SISSA (A.R.). Computer simulations discussed in this work were performed at Cineca (Bologna, Italy), CBP and PSMN (ENS-Lyon, France), and P2CHPD (UCB Lyon 1, France) by employing in part the equip@meso facilities of the FLMSN.

References

Alberts, B., et al., 2007. Molecular Biology of the Cell. fifth ed Garland Science, New York.
Allis, C., Jenuwein, T., Reinberg, D., 2007. Epigenetics. Cold Spring Harbor Laboratory Press, Cold Spring Harbor.
Barbieri, M., et al., 2012. Proc. Natl. Acad. Sci. U.S.A. 109, 16173.
Bates, F.S., Fredrickson, G.H., 1990. Annu. Rev. Phys. Chem. 41, 525.
Baù, D., et al., 2011. Nat. Struct. Mol. Biol. 18, 107.
Becker, N.B., Rosa, A., Everaers, R., 2010. Eur. Phys. J. E 32, 53.
Benedetti, F., Dorier, J., Burnier, Y., Stasiak, A., 2014. Nucleic Acids Res. 42, 2848.
Bennett, M.D., Leitch, I.J., 2005. In: Gregory, T.R. (Ed.), The Evolution of the Genome. Elsevier, San Diego, pp. 89–162.
Berger, A.B., et al., 2008. Nat. Methods 5, 1031.
Boettiger, A.N., et al., 2016. Nature 529, 418.
Bohn, M., Heermann, D.W., 2010. PLoS ONE 5, e12218.
Brackley, C.A., Johnson, J., Kelly, S., Cook, P.R., Marenduzzo, D., 2016. Nucleic Acids Res. 44, 3503.
Brereton, M.G., Vilgis, T.A., 1995. J. Phys. A: Math. Gen. 28, 1149.
Bystricky, K., Heun, P., Gehlen, L., Langowski, J., Gasser, S.M., 2004. Proc. Natl. Acad. Sci. U.S.A. 101, 16495.
Cabal, G.G., et al., 2006. Nature 441, 770.
Canzio, D., et al., 2013. Nature 496, 377.
Cates, M.E., Deutsch, J.M., 1986. J. Phys. (Paris) 47, 2121.
Cheutin, T., Cavalli, G., 2012. PLoS Genet. 8, e1002465.
Chiariello, A.M., Annunziatella, C., Bianco, S., Esposito, A., Nicodemi, M., 2016. Sci. Rep. 6, 29775.
Cook, P.R., 1999. Science 284, 1790.
Cook, P.R., 2010. J. Mol. Biol. 395, 1.
Cremer, T., Cremer, C., 2001. Nat. Rev. Genet. 2, 292.
Cremer, T., Cremer, C., 2006. Eur. J. Histochem. 50, 161.
Dekker, J., Marti-Renom, M.A., Mirny, L.A., 2013. Nat. Rev. Genet. 14, 390.
Dixon, J.R., et al., 2012. Nature 485, 376.
Dixon, J.R., et al., 2015. Nature 518, 331.
Dodd, I.B., Micheelsen, M.A., Sneppen, K., Thon, G., 2007. Cell 129, 813.
Doi, M., Edwards, S.F., 1986. The Theory of Polymer Dynamics. Oxford University Press, New York.
Doyle, B., Fudenberg, G., Imakaev, M., Mirny, L.A., 2014. PLoS Comput. Biol. 10, e1003867.
Edwards, S.F., 1967. Proc. Phys. Soc. 91, 513.
Emanuel, M., Radja, N.H., Henriksson, A., Schiessel, H., 2009. Phys. Biol. 6, 025008.
Fetters, L.J., Lohse, D.J., Richter, D., Witten, T.A., Zirkel, A., 1994. Macromolecules 27, 4639.
Florescu, A.-M., Therizols, P., Rosa, A., 2016. PLoS. Comput. Biol. 12, e1004987.
Fraser, J., et al., 2015a. Mol. Syst. Biol. 11, 852.
Fraser, J., Williamson, I., Bickmore, W.A., Dostie, J., 2015b. Microbiol. Mol. Biol. Rev. 79, 347.
Fudenberg, G., et al., 2016. Cell Rep. 15, 2038.

Ganai, N., Sengupta, S., Menon, G.I., 2014. Nucleic Acids Res. 42, 4145.
De Gennes, P.-G., 1971. J. Chem. Phys. 55, 572.
De Gennes, P.-G., 1979. Scaling Concepts in Polymer Physics. Cornell University Press, Ithaca.
Goloborodko, A., Imakaev, M.V., Marko, J.F., Mirny, L., 2016a. Elife 5, e14864.
Goloborodko, A., Marko, J.F., Mirny, L.A., 2016b. Biophys. J. 110, 2162.
Gregory, T.R., 2005. In: Gregory, T.R. (Ed.), The Evolution of the Genome. Elsevier, San Diego, pp. 3–87.
Grosberg, A., Rabin, Y., Havlin, S., Neer, A., 1993. Europhys. Lett. 23, 373.
Grosberg, A.Y., 2012. Polym. Sci. Ser. C 54, 1.
Grosberg, A.Y., 2014. Soft Matter 10, 560.
Grosberg, A.Y., Khokhlov, A.R., 1994. Statistical Physics of Macromolecules. AIP Press, New York.
Grosberg, A.Y., Nechaev, S.K., Shakhnovich, E.I., 1988. J. Phys. Fr. 49, 2095.
Guo, Y., et al., 2015. Cell 162, 900.
Haber, J.E., Leung, W.Y., 1996. Proc. Natl. Acad. Sci. U.S.A. 93, 13949.
Halverson, J.D., Lee, W.B., Grest, G.S., Grosberg, A.Y., Kremer, K., 2011. J. Chem. Phys. 134, 204904.
Halverson, J.D., Smrek, J., Kremer, K., Grosberg, A.Y., 2014. Rep. Prog. Phys. 77, 022601.
Heng, H.H.Q., et al., 1996. Proc. Natl. Acad. Sci. U.S.A. 93, 2795.
Heun, P., Laroche, T., Shimada, K., Furrer, P., Gasser, S.M., 2001. Science 293, 2181.
Hiragami-Hamada, K., et al., 2016. Nat. Commun. 7, 11310.
Ho, J.W.K., et al., 2014. Nature 512, 449.
Imakaev, M., et al., 2012. Nat. Methods 9, 999.
Isono, K., et al., 2013. Dev. Cell 26, 565.
Jerabek, H., Heermann, D.W., 2012. PLoS ONE 7, e37525.
Jost, D., 2014. Phys. Rev. E 89, 010701.
Jost, D., Carrivain, P., Cavalli, G., Vaillant, C., 2014. Nucleic Acids Res. 42, 9553.
Kavassalis, T.A., Noolandi, J., 1987. Phys. Rev. Lett. 59, 2674.
Khalil, A., et al., 2007. Chromosome Res. 15, 899.
Khokhlov, A.R., Nechaev, S.K., 1985. Phys. Lett. 112A, 156.
Klein, J., 1986. Macromolecules 19, 105.
Kratky, O., Porod, G., 1949. Recl. Trav. Chim. Pays-Bas. 68, 1106.
Kremer, K., Grest, G.S., 1990. J. Chem. Phys. 92, 5057.
Leitch, I.J., Soltis, D.E., Soltis, P.S., Bennett, M.D., 2005. Ann. Bot. 95, 207.
Lieberman-Aiden, E., et al., 2009. Science 326, 289.
Luger, K., Hansen, J.C., 2005. Curr. Opin. Struct. Biol. 15, 188.
Lukhtanov, V.A., 2015. Comp. Cytogenet. 9, 683.
Lupiáñez, D.G., et al., 2015. Cell 161, 1012.
Maeshima, K., Hihara, S., Eltsov, M., 2010. Curr. Opin. Cell Biol. 22, 291.
Mateos-Langerak, J., et al., 2009. Proc. Natl. Acad. Sci. U.S.A. 106, 3812.
McLeish, T.C.B., 2002. Adv. Phys. 51, 1379.
Mora, C., Tittensor, D.P., Adl, S., Simpson, A.G.B., Worm, B., 2011. PLoS Biol. 9, 1.
Müller, M., Wittmer, J.P., Cates, M.E., 1996. Phys. Rev. E 53, 5063.
Müller, M., Wittmer, J.P., Cates, M.E., 2000. Phys. Rev. E 61, 4078.
Münkel, C., et al., 1999. J. Mol. Biol. 285, 1053.
Naumova, N., et al., 2013. Science 342, 948.
Nazarov, L.I., Tamm, M.V., Avetisov, V.A., Nechaev, S.K., 2015. Soft Matter 11, 1019.
Nedelec, F.J., Surrey, T., Maggs, A.C., Leibler, S., 1997. Nature 389, 305.
Nora, E.P., et al., 2012. Nature 485, 381.
Obukhov, S.P., Rubinstein, M., Duke, T., 1994. Phys. Rev. Lett. 73, 1263.
Olarte-Plata, J.D., Haddad, N., Vaillant, C., Jost, D., 2016. Phys. Biol. 13, 026001.
Pederson, T., 2000. Mol. Biol. Cell 11, 799.

Pellicer, J., Fay, M.F., Leitch, I.J., 2010. Bot. J. Linn. Soc. 164, 10.
Prager, S., Frisch, H.L., 1967. J. Chem. Phys. 46, 1475.
Rabl, C., 1885. Morphol. Jahrb. 10, 214.
Ramalho, T., Selig, M., Gerland, U., Ensslin, T.A., 2013. Phys. Rev. E 87, 022719.
Rao, S.S.P., et al., 2014. Cell 159, 1665.
Rosa, A., Becker, N.B., Everaers, R., 2010. Biophys. J. 98, 2410.
Rosa, A., Everaers, R., 2008. PLoS Comput. Biol. 4, e1000153.
Rosa, A., Everaers, R., 2014. Phys. Rev. Lett. 112, 118302.
Rosa, A., Everaers, R., *J. Chem. Phys.* 145, 2016, 164906.
Rosa, A., Zimmer, C., 2014. Int. Rev. Cell Mol. Biol. 307, 275.
Rothemund, P.W.K., 2006. Nature 440, 297.
Rubinstein, M., 1986. Phys. Rev. Lett. 57, 3023.
Rubinstein, M., Colby, R.H., 2003. Polymer Physics. Oxford University Press, New York.
Sachs, R.K., van den Engh, G., Trask, B., Yokota, H., Hearst, J.E., 1995. Proc. Natl. Acad. Sci. U.S.A. 92, 2710.
Sanborn, A.L., et al., 2015. Proc. Natl. Acad. Sci. U.S.A. 112, E6456.
Sanyal, A., Lajoie, B.R., Jain, G., Dekker, J., 2012. Nature 489, 109.
Schram, R.D., Barkema, G.T., Schiessel, H., 2013. J. Chem. Phys. 138, 224901.
Sexton, T., et al., 2012. Cell 148, 458.
Sexton, T., Cavalli, G., 2015. Cell 160, 1049.
Shachar, S., Pegoraro, G., Misteli, T., 2015. Cold Spring Harb. Symp. Quant. Biol. 80, 73.
Sikorav, J.-L., Jannink, G., 1994. Biophys. J. 66, 827.
Sofueva, S., et al., 2013. EMBO J. 32, 3119.
Suzuki, J., Takano, A., Deguchi, T., Matsushita, Y., 2009. J. Chem. Phys. 131, 144902.
Tark-Dame, M., Jerabek, H., Manders, E.M.M., Heermann, D.W., van Driel, R., 2014. PLoS Comput. Biol. 10, e1003877.
Tiana, G., et al., 2016. Biophys. J. 110, 1234.
Tolhuis, B., et al., 2011. PLoS Genet. 7, e1001343.
Uchida, N., Grest, G.S., Everaers, R., 2008. J. Chem. Phys. 128, 044902.
Ulianov, S.V., et al., 2016. Genome Res. 26, 70.
Vettorel, T., Grosberg, A.Y., Kremer, K., 2009a. Phys. Biol. 6, 025013.
Vettorel, T., Grosberg, A.Y., Kremer, K., 2009b. Phys. Today 62, 72.
Weber, S.C., Spakowitz, A.J., Theriot, J.A., 2012. Proc. Natl. Acad. Sci. U.S.A., 109. p. 7338.
Weiland, Y., Lemmer, P., Cremer, C., 2011. Chromosome Res. 19, 5.
Wilkinson, D.J., 2009. Nat. Rev. Genet. 10, 122.
Wong, H., et al., 2012. Curr. Biol. 22, 1881.
Yao, J., Lowary, P.T., Widom, J., 1990. Proc. Natl. Acad. Sci. U.S.A. 87, 7603.
Zhu, Y., et al., 2016. Nat. Commun. 7, 10812.

This page intentionally left blank